Benzylamine-Treated Wide-Bandgap Perovskite with High Thermal-Photostability and Photovoltaic Performance

Zhou, Yang; Wang, Feng; Cao, Yu; Wang, Jian-Pu; Fang, Hong-Hua; Loi, Maria Antonietta; Zhao, Ni; Wong, Ching-Ping

Published in:
Advanced Energy Materials

DOI:
10.1002/aenm.201701048

Benzylamine-Treated Wide-Bandgap Perovskite with High Thermal-Photostability and Photovoltaic Performance

Yang Zhou, Feng Wang, Yu Cao, Jian-Pu Wang, Hong-Hua Fang, Maria Antonietta Loi, Ni Zhao, and Ching-Ping Wong**

Mixed iodide-bromide organolead perovskites with a bandgap of 1.70–1.80 eV have great potential to boost the efficiency of current silicon solar cells by forming a perovskite-silicon tandem structure. Yet, the stability of the perovskites under various application conditions, and in particular combined light and heat stress, is not well studied. Here, $FA_{0.15}Cs_{0.85}Pb(I_{0.73}Br_{0.27})_3$, with an optical bandgap of ≈1.72 eV, is used as a model system to investigate the thermal-photostability of wide-bandgap mixed halide perovskites. It is found that the concerted effect of heat and light can induce both phase segregation and decomposition in a pristine perovskite film. On the other hand, through a postdeposition film treatment with benzylamine (BA) molecules, the highly defective regions (e.g., film surface and grain boundaries) of the film can be well passivated, thus preventing the progression of decomposition or phase segregation in the film. Besides the stability improvement, the BA-modified perovskite solar cells also exhibit excellent photovoltaic performance, with the champion device reaching a power conversion efficiency of 18.1%, a stabilized power output efficiency of 17.1% and an open-circuit voltage (V_{oc}) of 1.24 V.

1. Introduction

Organic–inorganic hybrid perovskites (OIHPs) with a chemical structure of ABX_3 (where A is typically methylammonium (MA), formamidinium (FA) or Cs, B is Pb or Sn, and X is I, Br, or Cl) have recently emerged as a highly promising photovoltaic (PV) material, as they can be fabricated through low-cost solution processes while delivering high power conversion efficiency (PCE).[1–4] An attractive feature of the OIHPs is their tunable bandgap, ranging from 1.48 to 2.3 eV,[5,6] which is ideal for forming tandem cells with silicon or copper indium gallium (di)selenide.[7–9] In particular, the power conversion efficiency (PCE) of crystalline silicon solar cells has only been marginally improved during the last 15 years. Paring silicon with a low-cost wide-bandgap perovskite (WB-OIHP) to form a tandem solar cell could be a promising way to boost the PCE from 26.3%[10] (for single cells) to 30% (for tandem cells).[11,12]

Based on the requirement of current matching between the top and bottom cells of a tandem structure, a WB-OIHP with a bandgap of 1.7–1.8 eV should be used with silicon to achieve the maximum PCE.[13] Such bandgap can be easily achieved by using mixed bromide-iodide perovskites, e.g., $MAPbI_{2.2}Br_{0.8}$.[14] However, a common problem for the mixed halide perovskites is photoinduced phase segregation,[15] which occurs when the bromide ratio exceeds some threshold (e.g., $x > 0.2$ for $MAPb(I_{1-x}Br_x)_3$) and considerably degrades the PV performance and operation stability. It has been proposed that under light soaking halide ions migrate within the perovskite layer and form I-rich minority and Br-rich majority phases.[15] Several approaches have been explored to address this problem. Huang and co-workers utilized a hydrophobic surface to increase the grain size of $MAPbI_{2.2}Br_{0.8}$ (E_g = 1.75 eV), which has been shown to suppress the phase segregation and deliver a PCE of 14.9% and a high open-circuit voltage (V_{oc}) of 1.21 V.[14] More recently, Snaith et al. replaced MA with a mixture of FA and Cs at the *A* site of a 1.74 eV bandgap mixed-halide perovskite and demonstrated that the method can eliminate the light-induced phase segregation.[16] Besides achieving a solar cell with 17.1% PCE and 16% stabilized power output efficiency, they have also shown improved thermal stability in the mixed-cation system[16] as compared to $MAPb(I_{1-x}Br_x)_3$.[17]

It is noted that the aforementioned studies investigate the perovskite stability under either light soaking or heating, but not a combination of the two. On the other hand, in practical application conditions the temperature of solar panels can reach as high as 85 °C due to direct exposure of the solar panels to sunlight and local heating.[18] Since ion migration is thermally activated,[19] the photoinduced phase segregation may emerge at elevated temperatures. Therefore, to fully address

Y. Zhou, Prof. N. Zhao, Prof. C.-P. Wong
Department of Electronic Engineering
The Chinese University of Hong Kong
New Territories, Hong Kong
E-mail: nzhao@ee.cuhk.edu.hk; cpwong@cuhk.edu.hk
Dr. F. Wang
Department of Physics
Chemistry and Biology (IFM)
Linköping University
Linköping SE-58183, Sweden
Y. Cao, Prof. J.-P. Wang
Institute of Advanced Materials
Nanjing Tech University
210009 Nanjing, P. R. China
Dr. H.-H. Fang, Prof. M. A. Loi
Photophysics & OptoElectronics
Zernike Institute for Advanced Materials
Nijenborgh 4, Groningen, 9747 AG, The Netherlands

DOI: 10.1002/aenm.201701048

the stability issue of WB-OHIPs, the light-heat coupled effect should be taken into consideration.

In this work, we focus on the thermal-photostability of a WB-OIHP - $FA_{0.15}Cs_{0.85}Pb(I_{0.73}Br_{0.27})_3$, which has a similar bandgap (1.72 eV) as the previously reported WB-OIHP system for tandem cells.[16] We showed that the perovskite film exhibited decent photostability at room temperature (RT), but that the material underwent phase segregation, accompanied by decomposition, when it was light soaked at 85 °C. We further demonstrated that the thermal photoinduced degradation can be largely suppressed (i.e., no degradation after 8 h continuous light soaking at 85 °C) by a postdeposition treatment of the perovskite films with benzylamine (BA). Through a systematic investigation combining structure and morphology analysis and time- and spatial-resolved photoluminescence characterization, we revealed that the BA molecules could well passivate the defect states on both the film surface and grain boundaries. Furthermore, a partial proton transfer process occurred at the A sites of the top perovskite lattice, leading to the formation of 2D BA_2PbI_4 in some regions. The defect passivation together with the formation of the 2D/3D stacked structure effectively blocked the ion migration paths and removed the defect sites that could initiate decomposition and phase segregation. Remarkably, besides the stability improvement, the BA-OIHP based solar cells also showed excellent solar cell performance. The champion cell exhibited a stabilized power output efficiency of 17.1% and a high V_{oc} of 1.24 V. The BA-OIHP based cells maintained 80% of their original PCEs after 40 d exposure in ambient air with a humidity of 65 ± 5% RH, whereas the untreated devices degraded rapidly after 2 weeks.

2. Results and Discussion

The $Cs_{0.15}FA_{0.85}Pb(I_{0.73}Br_{0.27})_3$ thin film was fabricated through a one-step spin-coating process using chlorobenzene as an antisolvent. This method produces thin films with compact and uniform surface, as shown in **Figure 1**b. The films also possess good crystallinity, exhibiting two pronounced X-ray diffraction (XRD) peaks at $2\theta = 20.2°$ and 41.0° (Figure 1d), which correspond to the (110) and (220) lattice spacing of $Cs_{0.15}FA_{0.85}Pb(I_{0.73}Br_{0.27})_3$, respectively. The bandgap of the perovskite is measured to be 1.72 eV based on the Tauc plot (Figure S1, Supporting Information).

The BA molecules were introduced onto the perovskite film through spin-coating of a 2.5 vol% BA solution (in chlorobenzene) on the film. The top surface morphology of the perovskite film altered slightly after the spin-coating process (Figure S2, Supporting Information), and two small XRD peaks at $2\theta = 6.2°$ and 7.3° emerged (Figure 1d), indicating that some BA molecules may have intercalated into the perovskite lattice. The film was then annealed at 140 °C for 10 min. We previously found that this heating process can stabilize BA molecules on the perovskite surface.[20] The film morphology remained almost unchanged after the annealing process, except that some thin flake-like domains appeared on the film surface (Figure 1c). In the meanwhile, the XRD peak at 6.2° (Figure 1d) became prominent, which correspond well to the (200) diffraction of a 2D BA_2PbI_4 perovskite[21] (Figure 1d). We thus speculate that the flake-like domains are BA_2PbI_4 2D crystallites formed during the annealing process. The formation mechanism of these crystallites is discussed in Figures S3–S6

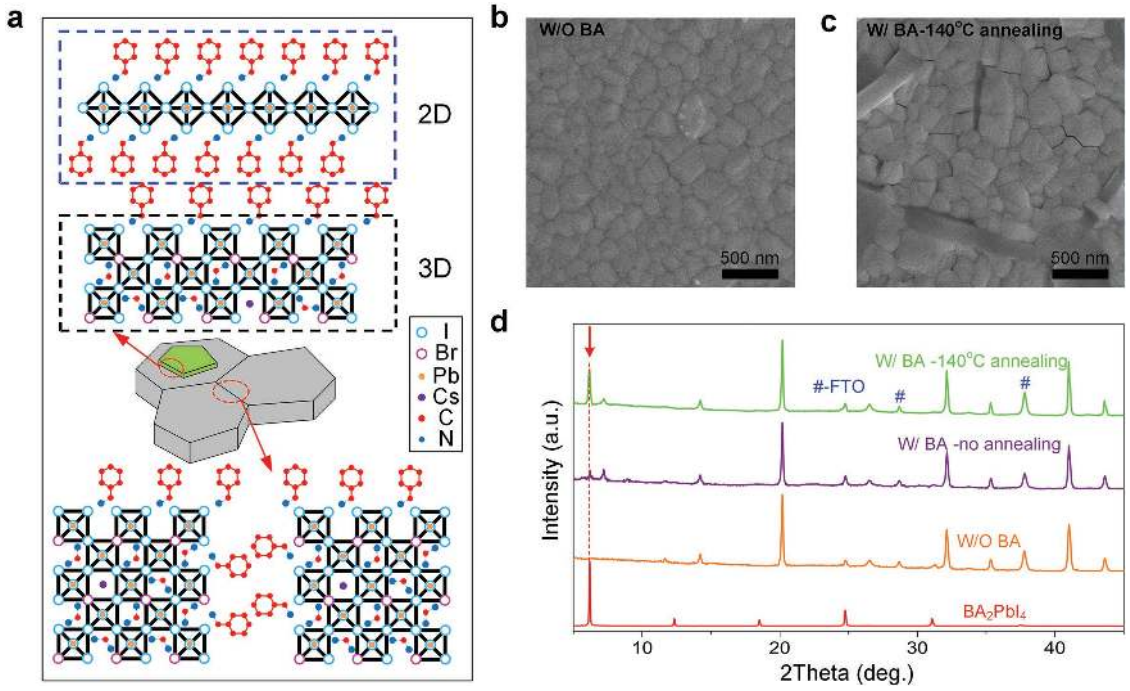

Figure 1. Structure and morphology modification with BA treatment. a) Schematic of the impact of BA modification on the $Cs_{0.15}FA_{0.85}Pb(I_{0.73}Br_{0.27})_3$ thin film, illustrating the surface and grain boundaries passivation and 2D BA_2PbI_4 formation. b) Surface morphology of the OIHP film W/O BA modification. c) Surface morphology of the OIHP film W/BA modification after annealing at 140 °C for 10 min, showing the formation of some crystallites on the top surface. d) XRD patterns evolution of the OIHP film during the BA treatment, showing the formation of 2D BA_2PbI_4 after annealing.

in the Supporting Information. Note that based on the XRD intensity change (Figure S6, Supporting Information) after the BA treatment, only a very small portion (less than 5%, see the Supporting Information for the detailed analysis) of the surface $Cs_{0.15}FA_{0.85}Pb(I_{0.73}Br_{0.27})_3$ was converted to BA_2PbI_4.

We first check separately the photostability and thermal-stability of the $Cs_{0.15}FA_{0.85}Pb(I_{0.73}Br_{0.27})_3$ perovskite films following the protocols used by others.[14,16] For the photostability test, the perovskite films with and without BA treatment (denoted as OIHP and BA-OIHP, respectively) were exposed to a continuous light excitation at 405 nm with an intensity of ≈30 mW cm^{-2}. At RT both the OIHP and BA-OIHP films maintain a stable photoluminescence (PL) emission after 10 min light excitation (Figure S7, Supporting Information). For the thermal stability test, the films were kept in dark and heated to 85 °C for 8 h and 130 °C for 8 h, respectively. The XRD patterns of the films were examined before and after the heat treatment. As shown in Figure S8 in the Supporting Information, the OIHP film exhibits no degradation after 8 h heating at 85 °C and only decomposes slightly after 8 h heating at 130 °C. The BA-OIHP film shows similar stability in this test.

The role of the BA treatment becomes significant when the light and heat effects are introduced to the films at the same time. Here, an accelerated aging test was conducted by heating the films to 85 °C while at the same time illuminating the samples with a 50 W white light emitting diode (LED) light source. The light intensity incident on the film surface is around 200 mW cm^{-2}. The emission spectrum of the LED is provided in Figure S10 in the Supporting Information. As shown in **Figure 2**a, after an 8 h aging test the OIHP thin film shows a distinct XRD signal of PbI_2 at $2\theta = 12.7°$, indicating decomposition of the OIHP thin film which may be due to partial elimination of Br. Furthermore, the main XRD peak at 20.20° splits to two peaks, one at 20.10° and the other at 21.10° (Figure 2a), due likely to a phase segregation process as previously observed in other mixed halide perovskites.[14,15] In contrast, the BA-OIHP thin film shows no PbI_2 XRD signal after the aging treatment; the main XRD peak of the film exhibits no splitting but only a very small shift from 20.20° to 20.16° (Figure 2a), suggesting that even though the phase segregation may still occur, it will evolve at a much slower rate. The PL emissions of the films were also examined. As shown in Figure 2b, aging induced 34 and 10 nm red-shift of the PL peaks of the OIHP and BA-OIHP films, respectively, corresponding to the formation of iodide-rich perovskite phases with lower bandgaps. Note that the iodide rich phases can form via phase segregation, partial

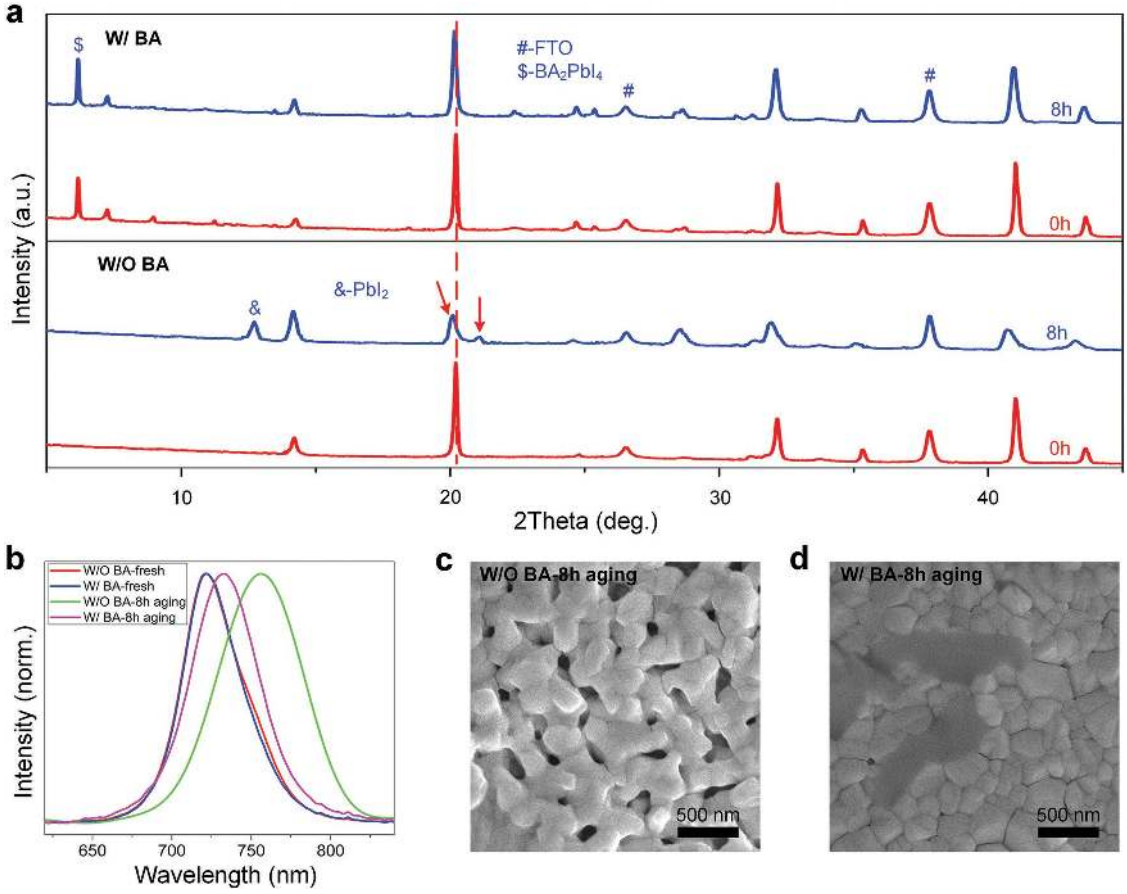

Figure 2. Investigation of the thermal-photostability of the $Cs_{0.15}FA_{0.85}Pb(I_{0.73}Br_{0.27})_3$ OIHP. a) XRD patterns of the OIHP and BA-OIHP aged 0 and 8 h under a white LED light source with an intensity of 200 mW cm^{-2} at 85 °C. b) The PL spectrum of the OIHP and BA-OIHP aged 0 and 8 h under a white LED light source with an intensity of 200 mW cm^{-2} at 85 °C. c) SEM image of the OIHP aged 8 h under a white LED light source with an intensity of 200 mW cm^{-2} at 85 °C. d) SEM image of the BA-OIHP aged 8 h under a white LED light source with an intensity of 200 mW cm^{-2} at 85 °C.

removal of bromide in the perovskite system, or combination of both. In addition, the PL intensity of the OIHP film is reduced by ≈40 times after aging, while the intensity reduction is only 41% for the BA-OIHP film (Figure S12, Supporting Information). Both the XRD and PL results suggest that the BA treatment effectively suppresses the decomposition and phase segregation processes during aging. We also observed that the aged OIHP film exhibits pronounced change in its morphology (Figure 2c), with voids developed at the grain boundaries (GBs) of the film. The result indicates that the film decomposition may initiate from the film surface and GBs, where a large number of defects are present. With BA passivation the perovskite film exhibits almost no morphological change after aging (Figure 2d), demonstrating that the BA molecules can prevent the progression of decomposition from film surfaces or GBs. We have also examined the efficacy of the BA treatment on other $Cs_{0.15}FA_{0.85}Pb(I_xBr_{1-x})_3$ systems, including $x = 0.15$, $x = 0.4$, and $x = 0.6$, and found that all the systems exhibited improved thermal-photostability after BA modification (Figures S13 and S14, Supporting Information).

To correlate the film morphology with the optical property, we performed PL mapping on the fresh and aged OIHP and BA-OIHP thin films. The fresh OIHP film shows bright and uniform PL emission across the surface (**Figure 3**a), while the aged OIHP film turns almost to dark in the PL map plotted with the same color scale (Figure 3b). The much weakened PL emission is likely associated with the nonradiative recombination centers induced by decomposition and phase segregation. In contrast, the PL image of the BA-OIHP film exhibits a much smaller variation in its brightness before and after aging (Figure 3c,d), consistent with the XRD and scanning electron microscopy (SEM) results. Interestingly, the PL emission of the fresh BA-OIHP film (Figure 3c) is less uniform than that of the fresh OIHP film (Figure 3a). We speculate that this is related to the coexistence of two surface passivation mechanisms: On one hand, part of the OIHP surface is covered with 2D BA_2PbI_4 after BA treatment; the 2D perovskite can form a type-II heterojunction with the 3D perovskite underneath (Figure 3e) and thus quench the PL emission,[22,23] resulting in less bright regions in the PL image. (The energy levels in Figure 3e were derived from the ultraviolet photonelectron spectroscopy (UPS) measurement as shown in Figure S15 in the Supporting Information.) On the other hand, the surface regions without 2D perovskite coverage, but well passivated by BA, can emit at the same or even higher PL intensity level than the fresh OIHP film (Figure 3a,c). In general, the overall time-resolved PL (TRPL) decay of the fresh BA-OIHP film is slightly faster than that of the OIHP film (Figure 3f). The presence of the 2D perovskite can help hole extraction from the bulk 3D perovskite while impeding the electron transport, thus reducing charge recombination loss at the perovskite top surface.

Perovskite solar cells were fabricated using an fluorine-doped tin oxide (FTO)/compact TiO_2 (c-TiO_2)/perovskite/2,2′,7,7′-tetrakis[N,N-di(4-methoxyphenyl)amino]-9,9′-spirobifluorene (spiro-MeOTAD)/Au structure. We found that the device performance and stability were greatly improved after BA modification. **Figure 4**a shows the device statistics (including open circuit voltage (V_{oc}), short circuit current (J_{sc}), fill factor (FF), and PCE of 28 OIHP devices and 46 BA-OIHP devices collected over 8 different fabrication batches. It can be seen that the

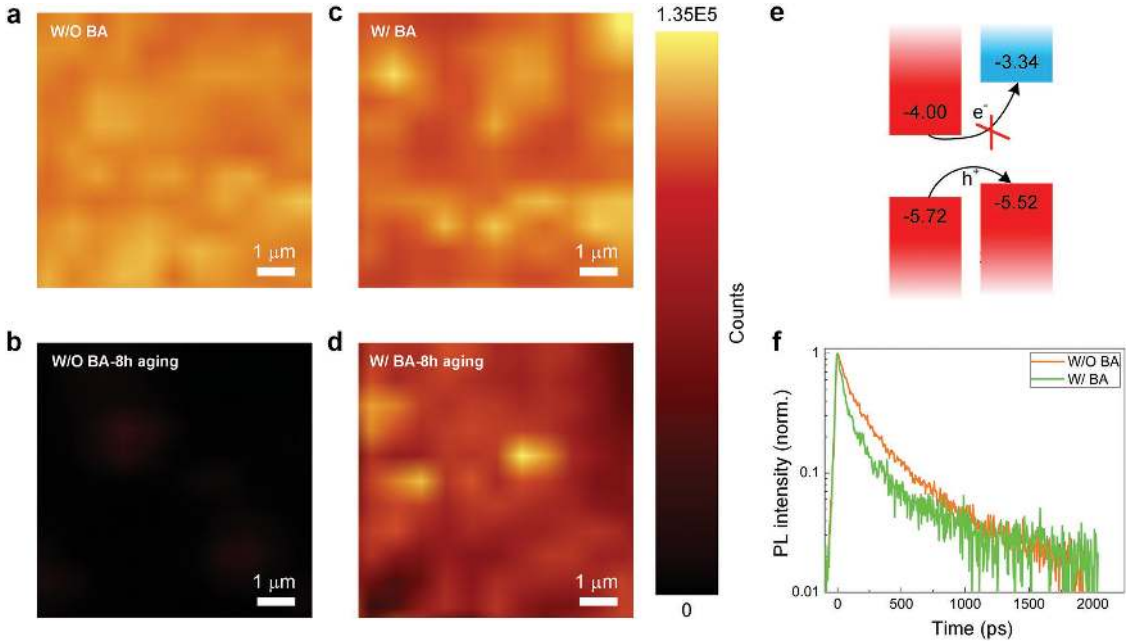

Figure 3. Investigation of the impact of BA modification on the thermal-photostability and carriers' transportation. a) PL mapping image of the fresh OIHP. b) PL mapping image of the OIHP aged 8 h under a white LED light source with an intensity of 200 mW cm^{-2} at 85 °C. c) PL mapping image of the fresh BA-OIHP. d) PL mapping image of the BA-OIHP aged 8 h under a white LED light source with an intensity of 200 mW cm^{-2} at 85 °C. Note that since the samples were removed from the microscope stage for the aging treatment, the imaging regions of the fresh and aged samples were not identical. We, however, examined multiple regions and ensured that the figures shown are representative for the entire films tested. e) Role of BA_2PbI_4 in extracting the holes and blocking the electrons. f) TRPL decays of the OIHP and BA-OIHP thin films prepared on glass substrate.

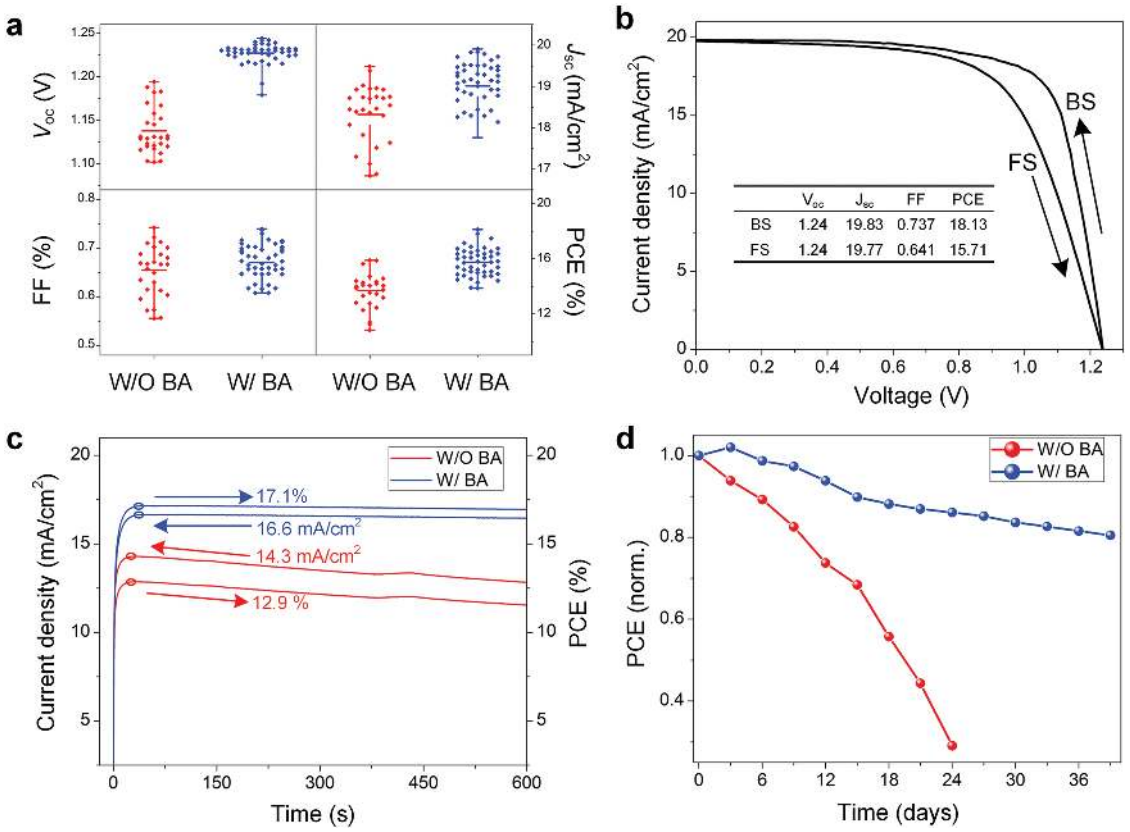

Figure 4. Improvement of PV performance and stability by BA modification. a) Statistics of V_{oc}, J_{sc}, FF, and PCE of 28 OIHP devices and 46 BA-OIHP devices collected over 8 different batches. b) *J–V* curve of the champion device using BA-OIHP as the light absorber. c) Power outputs of the BA-OIHP champion device and the OIHP device measured at the maximum output point of 1.03 and 0.9 V, respectively. d) Ambient stability test of the OIHP and BA-OIHP devices. The devices were unencapsulated and exposed in the air with a humidity of 65 ± 5% RH at room temperature.

BA-OIHP devices show improvement in both the average values and standard deviations for all device parameters. Particularly, the V_{oc} of the BA-OIHP devices (1.227 ± 0.012 V) is considerably higher than that of the OIHP devices (1.138 ± 0.026 V) (Figure 4a). Considering that the energy bandgap of OIHP is 1.72 eV (Figure S1, Supporting Information), the loss-in-potential of the champion BA-OIHP cell (with a V_{oc} of 1.24 V) is only 0.48 eV. The raised V_{oc} by BA treatment can be attributed to the suppressed phase segregation through BA modification and the reduced charge recombination in the GBs and interfaces,[20] as indicated by the higher shunt resistance of the BA-OIHP device (168 ± 13 kΩ) as compared to the OIHP device (68 ± 14 kΩ). The champion BA-OIHP solar cell shows a backward scan PCE of 18.1% (Figure 4b) and a stabilized power output efficiency of 17.1% measured over a 600 s period. In contrast, the power output of the untreated OIHP solar cell shows obvious decay within 600 s (Figure 4c). The high stabilized power output efficiency manifests the effectiveness of BA modification in improving the operation stability of WB-OIHP based solar cells. Furthermore, the BA-OIHP solar cell remains 80% of the PCE after 40 d exposure (Figure 4d) in ambient air with a humidity of 65 ± 5% RH (note that the degradation may be caused by the doped Spiro-MeOTAD layer);[20] whereas the OIHP devices without BA treatment degrade by more than 70% after 3 weeks.

3. Conclusions

In conclusion, we have investigated the thermal-photostability of a wide-bandgap perovskite, $Cs_{0.15}FA_{0.85}Pb(I_{0.73}Br_{0.27})_3$, and demonstrated an effective way of improving the stability of the film with BA treatment. We found that the concerted effect of heat and light can induce both phase segregation and decomposition in the untreated perovskite films. Through BA modification, the highly defective regions (e.g., film surface and grain boundaries) can be well passivated, thus preventing the progression of decomposition or phase segregation in the film. Apart from surface passivation, we also found that BA molecules can react with the perovskite in part of its surface area to form a thin 2D BA_2PbI_4. The 2D layer and its underneath 3D perovskite creates an energy cascade, which facilitates hole extraction to the top hole transport layer while blocking electron transport. The device performance as well as the ambient stability of the perovskite solar cells are greatly improved after the BA modification. The champion BA-OIHP solar cell exhibits a V_{oc} of 1.24 V and a stabilized power output efficiency of 17.1% under 1 sun illumination, both being the highest for ≈1.72 eV bandgap perovskite solar cells. This study elucidates the molecular passivation principles to achieve high thermal-photostability for wide-bandgap mixed halide perovskites, which is

critical for preserving the high performance of perovskite-based tandem cells in practical application conditions.

4. Experimental Section

Perovskite Thin Film and Solar Cell Fabrication: Nippon sheet glass was cleaned by sonication in a 2% Hellmanex water solution for 30 min. After rinsing with deionized water and ethanol, the substrates were further cleaned with isopropanol, acetone, and isopropanol for 30 min, respectively. Then, the TiO_2 precursor solution was prepared by dissolving 0.3 M titanium isopropoxide (Sigma-Aldrich, 99.999%) and 0.01 M HCl in ethanol. An ≈40 nm thick compact TiO_2 film was coated on the FTO substrate by spinning the precursor solution at 5000 rpm, followed by annealing at 500 °C for 30 min. 0.85 M formamidinium iodide (FAI, Dyesol), 0.15 M CsI (Sigma-Aldrich, 99.999%), 0.6 M PbI_2 (Sigma-Aldrich, 99%), and 0.4 M $PbBr_2$ (Sigma-Aldrich, 99.999%) were mixed in anhydrous N,N-Dimethylformamide (DMF):Dimethyl sulfoxide (DMSO) 9:1 (v:v), stirred overnight. The precursor solution was spin-coated onto the TiO_2/FTO substrates in a two-step procedure at 500 and 5000 rpm for 2 and 40 s, respectively. During the second step, 60 µL of chlorobenzene was casted onto the substrate 3 s after the beginning of the second spinning step. The films were placed on a hotplate at 100 °C for 10 min and at 140 °C for 30 min. For the benzylamine modification, 30 µL of 2.5 vol% benzylamine (Sigma-Aldrich, 99.0%) solution in chlorobenzene was dropped onto the perovskite surface, immediately followed by spinning coating at 3000 rpm for 60 s and then annealing at 140 °C for 10 min to completely remove the solvent. The perovskite thin films for photostability test were sealed and soaked under a 405 nm laser with an intensity of 30 mW cm^{-2} in air. The perovskite thin films for thermal-photostability test were stressed under a white light LED (Philip BVP161, 50 W, color temperature 5500 K) at 85 °C on a hotplate in the N_2 atmosphere. The incident light intensity on the films' surface was tuned to be ≈200 mW cm^{-2} by adjusting the distance between the surface of the LED light source and the sample. The intensity was monitored by a solar meter. The spiro-MeOTAD covered perovskite films for thermal-light stability test were prepared by spin-coating of 10 mg mL^{-1} spiro-MeOTAD solution in chlorobenzene at 4000 rpm for 30 s. After the heat-light stressing, the spiro-MeOTAD layer was washed away by chlorobenzene for XRD and PL measurement. The hole-transport layer was prepared by (1) dissolving 72.3 mg spiro-MeOTAD (TRC, Canada), 28 µL 4-tert-butylpyridine (Sigma-Aldrich, 96%), and 17.5 µL bis(trifluoromethane)sulfonimide lithium salt (Sigma-Aldrich) solution (520 mg Li-TFSI in 1 mL acetonitrile) in 1 mL chlorobenzene, and (2) spin-casting the solution on the perovskite layer at 4000 rpm for 30 s. Finally, a 100 nm Au electrode layer was deposited under a vacuum of $<1 \times 10^{-4}$ Pa with a rate of 0.1 nm s^{-1}. All fabrication steps were performed in a N_2-purged glove box.

Measurement and Characterization: UV–vis absorption spectra were taken on a Hitachi U-3501 ultraviolet/visible/near-infrared spectrophotometer. The XRD patterns of the samples were recorded using a Rigaku RU-300 diffractometer equipped with Cu $K\alpha_1$ irradiation (λ = 1.5406 Å). The film morphology was characterized using SEM (Quanta 400). Sample thicknesses were measured using an Alpha-step 500 surface profiler. The current density–voltage (*J–V*) curves were measured under simulated AM 1.5 sunlight (94011A-ES, ABB) at a scan rate of about 0.1 V s^{-1}. The effective area of a cell was 0.05 cm^2. Time-resolved photoluminescence measurements (TRPL) were performed by exciting the samples with the second harmonic (400 nm) of a mode-locked femtosecond Ti:Sapphire laser with a repetition rate of 76 MHz (Mira 900, Coherent). The excitation density was reduced to be 1.4 µJ cm^{-2} by a neutral density filter for TRPL measurements. The spectra were detected using a Hamamatsu streak camera. The PL spectra were measured by a AvaSpec ULS2048 × 64 (Avantes), under the excitation of 405 nm light source with an intensity of ≈30 mW cm^{-2}. The PL mapping was recorded by a WITec alpha 300R confocal Raman microscope, excited by a 635 nm laser with a power of ≈2.4 µW.

Supporting Information

Supporting Information is available from the Wiley Online Library or from the author.

Acknowledgements

The authors gratefully acknowledge the funding from the Theme-based Research Scheme (Grant No. T23-407/13-N) from the Research Grants Council of Hong Kong.

Conflict of Interest

The authors declare no conflict of interest.

Keywords

passivation, photostability, solar cells, thermal stability, wide-bandgap perovskites

Received: April 16, 2017
Revised: June 28, 2017
Published online: September 1, 2017

[1] A. Kojima, K. Teshima, Y. Shirai, T. Miyasaka, *J. Am. Chem. Soc.* **2009**, *131*, 6050.
[2] H. Kim, C. Lee, J. Im, K. Lee, T. Moehl, A. Marchioro, S. Moon, R. Humphry-Baker, J. Yum, J. E. Moser, *Sci. Rep.* **2012**, *2*, 591.
[3] N. J. Jeon, J. H. Noh, W. S. Yang, Y. C. Kim, S. Ryu, J. Seo, S. I. Seok, *Nature* **2015**, *517*, 476.
[4] M. Saliba, T. Matsui, K. Domanski, J. Seo, A. Ummadisingu, S. M. Zakeeruddin, J. Correa-Baena, W. R. Tress, A. Abate, A. Hagfeldt, *Science* **2016**, *354*, 206.
[5] J. H. Noh, S. H. Im, J. H. Heo, T. N. Mandal, S. I. Seok, *Nano Lett.* **2013**, *13*, 1764.
[6] G. E. Eperon, S. D. Stranks, C. Menelaou, M. B. Johnston, L. M. Herz, H. J. Snaith, *Energy Environ. Sci.* **2014**, *7*, 982.
[7] T. Todorov, T. Gershon, O. Gunawan, Y. S. Lee, C. Sturdevant, L. Y. Chang, S. Guha, *Adv. Energy Mater.* **2015**, *5*, 1500799.
[8] J. Werner, C. Weng, A. Walter, L. Fesquet, J. P. Seif, S. De Wolf, B. Niesen, C. Ballif, *J. Phys. Chem. Lett.* **2016**, *7*, 161.
[9] G. E. Eperon, T. Leijtens, K. A. Bush, R. Prasanna, T. Green, J. T. Wang, D. P. McMeekin, G. Volonakis, R. L. Milot, R. May, *Science* **2016**, *354*, 861.
[10] K. Yoshikawa, H. Kawasaki, W. Yoshida, T. Irie, K. Konishi, K. Nakano, T. Uto, D. Adachi, M. Kanematsu, H. Uzu, *Nat. Energy* **2017**, *2*, 17032.
[11] V. Sivaram, S. D. Stranks, H. J. Snaith, *Sci. Am.* **2015**, *313*, 54.
[12] M. A. Green, K. Emery, Y. Hishikawa, W. Warta, E. D. Dunlop, *Prog. Photovoltaics* **2015**, *23*, 805.
[13] C. R. Kagan, D. B. Mitzi, C. D. Dimitrakopoulos, *Science* **1999**, *286*, 945.

[14] M. Hu, C. Bi, Y. Yuan, Y. Bai, J. Huang, *Adv. Sci.* **2015**, *3*, 1500301.
[15] E. T. Hoke, D. J. Slotcavage, E. R. Dohner, A. R. Bowring, H. I. Karunadasa, M. D. McGehee, *Chem. Sci.* **2015**, *6*, 613.
[16] D. P. McMeekin, G. Sadoughi, W. Rehman, G. E. Eperon, M. Saliba, M. T. Hörantner, A. Haghighirad, N. Sakai, L. Korte, B. Rech, M. B. Johnston, L. M. Hertz, H. J. Snaith, *Science* **2016**, *351*, 151.
[17] B. Conings, J. Drijkoningen, N. Gauquelin, A. Babayigit, J. D'Haen, L. D'Olieslaeger, A. Ethirajan, J. Verbeeck, J. Manca, E. Mosconi, *Adv. Energy Mater.* **2015**, *5*, 1500477.
[18] R. G. Ross Jr., M. I. Smokler, Jet Propulsion Lab., Pasadena, CA, USA **1986**.
[19] Y. Shao, Y. Fang, T. Li, Q. Wang, Q. Dong, Y. Deng, Y. Yuan, H. Wei, M. Wang, A. Gruverman, *Energy Environ. Sci.* **2016**, *9*, 1752.
[20] F. Wang, W. Geng, Y. Zhou, H. H. Fang, C. J. Tong, M. A. Loi, L. M. Liu, N. Zhao, *Adv. Mater.* **2016**, *28*, 9986.
[21] L. Mao, H. Tsai, W. Nie, L. Ma, J. Im, C. C. Stoumpos, C. D. Malliakas, F. Hao, M. R. Wasielewski, A. D. Mohite, *Chem. Mater.* **2016**, *28*, 7781.
[22] M. Yuan, L. N. Quan, R. Comin, G. Walters, R. Sabatini, O. Voznyy, S. Hoogland, Y. Zhao, E. M. Beauregard, P. Kanjanaboos, *Nat. Nanotechnol.* **2016**, *11*, 872.
[23] Y. Hu, J. Schlipf, M. Wussler, M. L. Petrus, W. Jaegermann, T. Bein, P. Muller-Buschbaum, P. Docampo, *ACS Nano* **2016**, *10*, 5999.

